

Article

High Sensitivity Refractometer Based on TiO₂-Coated Adiabatic Tapered Optical Fiber via ALD Technology

Shan Zhu ¹, Fufei Pang ^{1,*}, Sujuan Huang ¹, Fang Zou ^{1,2}, Qiang Guo ¹, Jianxiang Wen ¹ and Tingyun Wang ¹

¹ Key Laboratory of Specialty Fiber Optics and Optical Access Networks, Shanghai University, 149 Yanchang Road, Shanghai 200072, China; ss_zhu@shu.edu.cn (S.Z.); sjhuang@shu.edu.cn (S.H.); zf-198166@sohu.com (F.Z.); qguo@staff.shu.edu.cn (Q.G.); wenjx@shu.edu.cn (J.W.); tywang@shu.edu.cn (T.W.)

² Hebei GEO University, 136 East Huaian Road, Shijiazhuang 050031, China

* Correspondence: ffpang@shu.edu.cn; Tel.: +86-21-5638-8746

Academic Editor: W. Rudolf Seitz

Received: 25 May 2016; Accepted: 10 August 2016; Published: 15 August 2016

Abstract: Atomic layer deposition (ALD) technology is introduced to fabricate a high sensitivity refractometer based on an adiabatic tapered optical fiber. Different thicknesses of titanium dioxide (TiO₂) nanofilm were coated around the tapered fiber precisely and uniformly under different deposition cycles. Attributed to the higher refractive index of the TiO₂ nanofilm compared to that of silica, an asymmetric Fabry–Perot (F-P) resonator could be constructed along the fiber taper. The central wavelength of the F-P resonator could be controlled by adjusting the thickness of the TiO₂ nanofilm. Such a F-P resonator is sensitive to changes in the surrounding refractive index (SRI), which is utilized to realize a high sensitivity refractometer. The refractometer developed by depositing 50.9-nm-thickness TiO₂ on the tapered fiber shows SRI sensitivity as high as 7096 nm/RIU in the SRI range of 1.3373–1.3500. Due to TiO₂'s advantages of high refractive index, lack of toxicity, and good biocompatibility, this refractometer is expected to have wide applications in the biochemical sensing field.

Keywords: refractometer; adiabatic tapered optical fiber; titanium dioxide nanofilm; atomic layer deposition

1. Introduction

Optical fiber refractometers are of great importance to the biochemical sensing field due to the advantages of high sensitivity, compact size, and anti-electromagnetic interference. For most of the fiber-based refractometers, the response of the sensor to changes in surrounding refractive index (SRI) is nonlinear, in which the sensitivity is much higher for an SRI close to 1.45 (which is the fiber material refractive index), but lower for an SRI close to 1.33 [1,2]. In order to improve SRI sensitivity in the vicinity of an SRI of 1.33 (which is the environment refractive index of the most of biosensors), nanofilm-coated optical fibers with metallic materials, semiconductor materials or high refractive index dielectric materials have been widely investigated [3–13]. One strategy is the deposition of high refractive index nanofilm on fibers which exhibit a mode resonant feature. These fibers include long period gratings (LPGs) fiber [3–5], double cladding fiber (DCF) [6], and cascading single-mode–multi-mode–single-mode (SMS) fiber [7]. It has been demonstrated that the sensitivity of these SRI sensors can be enhanced by mode reorganization behavior. However, since the SRI sensitivity can only be improved significantly in the transition region, the enhancement is limited. Hence, the schemes based on fibers without mode resonant feature are developed, including adiabatic tapered optical fiber, D-shaped optical fiber, cladding-removed multimode optical fiber, etc. Depending on the

properties of the nanofilm, these fiber-optic refractometers without mode resonance work based on either surface Plasmon resonance (SPR) [8,9] or lossy modes resonance (LMR) [10–13]. For SPR-based refractometers, the real part of the permittivity of the coated nanofilm is negative and higher in magnitude than both its own imaginary part and the permittivity of the material surrounding the nanofilm. In this case, the evanescent wave in the fiber is coupled to the surface Plasmon polariton. For LMR-based refractometers, the fiber is coated by high refractive index-absorbing nanofilm, whose real part of permittivity is positive and higher in magnitude than both its own imaginary part and the permittivity of the material surrounding the nanofilm, such as indium tin oxide (ITO) [10,11], titanium dioxide (TiO_2) [12], aluminum oxide (Al_2O_3) [13], and $[\text{PAH-PAA}]_x$ polymeric thin film [14]. Light guided in these structures is coupled to the lossy mode in the nanofilm. LMR has the advantage that it can be generated using a wide variety of materials in a wide spectral range.

The common technologies used to deposit nanofilms on optical fiber include dip-coating method [15], self-assembly method [12,14], sputtering technique [10,11], etc. However, precise control of film thickness cannot be achieved by dip-coating method. Self-assembly method requires the precise control of external parameters (pressure, humidity, temperature, etc.) to produce homogeneous and repetitive nanofilm. For sputtering technique, it is difficult to form a uniform nanofilm around the fiber's cylindrical surface. Recently, atomic layer deposition (ALD) technology is considered to be one of the most promising nanofilm deposition techniques in optical fiber fields [16]. ALD technology is a conformal deposition process through sequential, self-limiting surface reactions. Compared with conventional fiber coating technologies, ALD technology has special advantages, including accurate thickness control, good conformity for complex shapes, excellent step coverage, and good uniformity and adhesion. Many studies have shown that ALD is very suitable for coating a nanofilm on the rod shape of an optical fiber to realize functional fiber components [13,17–19].

Adiabatic tapered optical fiber sensors have been studied in previous work by coating Al_2O_3 via ALD technology. It was demonstrated that SRI sensitivity can be improved by coating with nanofilms with higher refractive indices [13]. TiO_2 has a higher refractive index than Al_2O_3 , with advantages such as lack of toxicity and good biocompatibility, making it more suitable for biochemical sensing. In this paper, we have experimentally demonstrated that TiO_2 can be coated on tapered optical fiber by using ALD technology for high sensitivity refractometers. Theoretical analysis is also conducted based on ray optics to explain the interference resonance inside the fiber. The optical field confined in the tapered fiber leaks out into the nanofilm, and multiple beam interference occurs, which can be regarded as a thin film Fabry–Perot (F-P) resonator. Its resonant transmission spectrum depends strongly on the SRI variation, which allows the detection of SRI with high sensitivity. The refractometer developed by depositing 50.9-nm-thickness TiO_2 on the tapered fiber shows an SRI sensitivity of 7096 nm/RIU in the SRI range of 1.3373–1.3500.

2. Theory

To simulate a sensor based on an adiabatic tapered optical fiber with a high refractive index nanofilm as shown in Figure 1, a theoretical model was developed, and the applicability of this method has been proven successfully in [13] for Al_2O_3 -coated tapered optical fiber. For the adiabatic tapered fiber with a uniform waist, the transmission loss is almost negligible because of the weak energy of the excited high-order modes, and only fundamental mode is considered to propagate in the taper waist section [20]. Therefore, the theoretical model of the tapered fiber sensor can be simplified to be a nanofilm-coated cylindrical waveguide with infinite surrounding, where r refers to diameter, L refers to length, d refers to nanofilm thickness, n_3 refers to SRI, as shown in Figure 1b,c. Since the nanofilm refractive index is higher than that of the fiber taper, light waves cannot be confined in the fiber by total internal reflection (TIR). As depicted in Figure 1b, when the light strikes on the taper–nanofilm interface with grazing incidence, the light will be partially reflected, and then be completely reflected at the nanofilm–surrounding interface. As a result, multiple beam interference

occurs along the tapered fiber, just like a thin film F-P interferometer. The transmission will present a periodic interference spectrum.

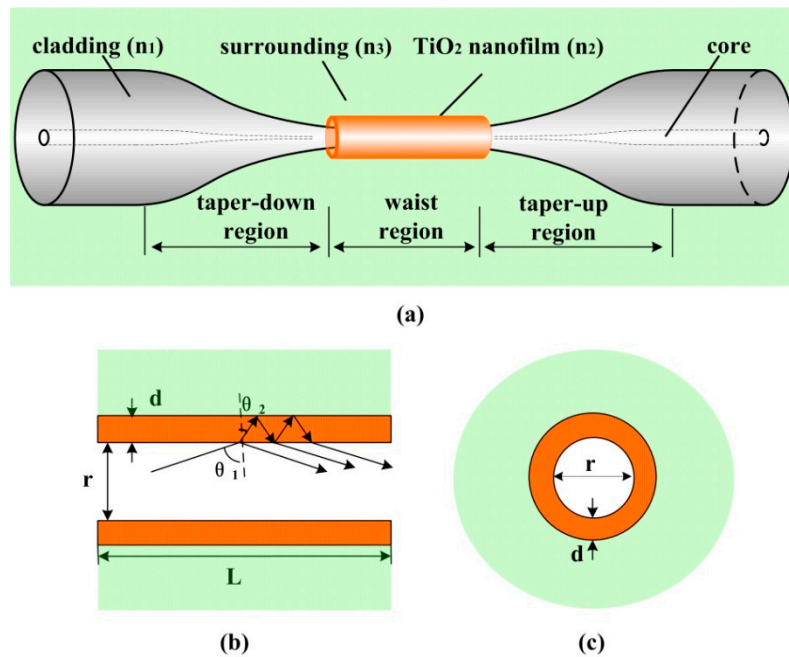


Figure 1. Schematic diagram of (a) the tapered fiber coated with TiO₂ nanofilm, and the coated region in the (b) axial and (c) radial directions.

If the propagation light wave in the fiber taper is not polarized, the combination of the reflected power in s and p polarization should be taken into account. The light path presents a zigzag ray trajectory due to multiple reflections on the taper-nanofilm interface. The general expression for the transmission is [21]

$$P = \left[\frac{1}{2} |F_s(\lambda)|^2 + \frac{1}{2} |F_p(\lambda)|^2 \right]^N \quad (1)$$

F_s and F_p can be described as [22]

$$F_s = \frac{r_{s1} + r_{s2} \exp(i\sigma)}{1 + r_{s1} r_{s2} \exp(i\sigma)} \quad (2)$$

$$F_p = \frac{r_{p1} + r_{p2} \exp(i\sigma)}{1 + r_{p1} r_{p2} \exp(i\sigma)} \quad (3)$$

where r_{s1} and r_{p1} are the Fresnel coefficients for s and p polarization of the taper-nanofilm interface, and r_{s2} and r_{p2} are the Fresnel coefficients for s and p polarization of the nanofilm-surrounding interface, respectively. $\sigma = 4\pi n_2 d \cos\theta_2 \lambda^{-1}$ is the phase delay induced by optical path difference, n_2 is the nanofilm refractive index, θ_2 is the incidence angle on the nanofilm-surrounding interface. If the nanofilm is lossy, its refractive index becomes a complex one. $N = L / (r \tan\theta_1)$ is the number of reflections at the taper-nanofilm interface, and θ_1 is the incidence angle on the taper-nanofilm interface. For the fundamental mode, can be expressed by $\theta_1 = \arcsin(\beta_{HE11} / (k_0 n_1))$, where $k_0 = 2\pi / \lambda$, β_{HE11} is the propagation constant of the fundamental mode, and n_1 is the cladding refractive index.

Since each incident angle corresponds to a fixed wavelength for the fundamental mode, the transmission presents interference dips at different wavelengths, as follows [23]:

$$\lambda_m = \frac{4\pi n_2 d \cos\theta_2}{\phi + 2m\pi} \quad (4)$$

where ϕ is the phase delay induced by the Goos–Hänchen shift due to the TIR on the nanofilm–surrounding interface, $\phi = 2\arctan\left(\sqrt{2\Delta\cos\theta_2^{-2}-1}\right)$ is for s polarization, $\phi = 2\arctan\left(n_2^2n_3^{-2}\sqrt{2\Delta\cos\theta_2^{-2}-1}\right)$ is for p polarization, and $\Delta = \frac{1}{2}\frac{n_2^2-n_3^2}{n_2^2}$. It is obvious that the dips will shift as a function of the nanofilm thickness, the nanofilm refractive index, and the SRI from Equation (4). When the nanofilm thickness and refractive index are defined, the SRI sensing can be realized by monitoring the shifts of the dips.

Simulation results using the above model are presented in Figures 2 and 3. In the simulation, material dispersion of refractive index for the TiO₂ nanofilm was referred from [24] ($n_{\text{TiO}_2} \approx 2.278$ @ 1550 nm), and the imaginary part was set as 0.005. The waist diameter and length are 25 μm and 7 mm, respectively. In Figure 2, there are multiple resonant dips generated by the asymmetric F-P resonator. The m th resonant pairs correspond to different polarization transmission, which has been demonstrated in [13]. These resonant spectra present red shift and bandwidth broadening with the increase of the nanofilm thickness, and the low order resonant spectrum shifts faster than the high order one. Attributed to the spectral dependency of the nanofilm, the resonant wavelength can be tuned from the visible to the near-infrared wavelength band. For a definite nanofilm material, it is possible to tune the resonant dip conveniently by changing the nanofilm thickness.

As shown in Figure 3, we observe that the resonant wavelengths shift to longer wavelength as the SRI increases. According to Equation (4), when the nanofilm refractive index and thickness are defined, the variation of SRI causes r_{s2} and r_{p2} of the nanofilm–surrounding interface to change. As a result, the phase delay induced by the Goos–Hänchen shift changes, which leads to the shift of the transmission interference spectrum. Moreover, it can be found that the wavelength shift of the 0th s polarization resonant dip is larger than others; namely, the sensitivity of the 0th s polarization resonant dip is highest [13]. Hence, we only focus on the 0th s polarization resonant dip in the following work. By monitoring the shift of the 0th s polarization resonant dip, the change of the SRI can be obtained. Additionally, in Figure 2, the 0th s polarization resonant dip sweeps the range 500 nm–2000 nm between thickness 10 nm and 60 nm. Therefore, the resonant wavelength position (working point) can be controlled by changing the nanofilm thickness.

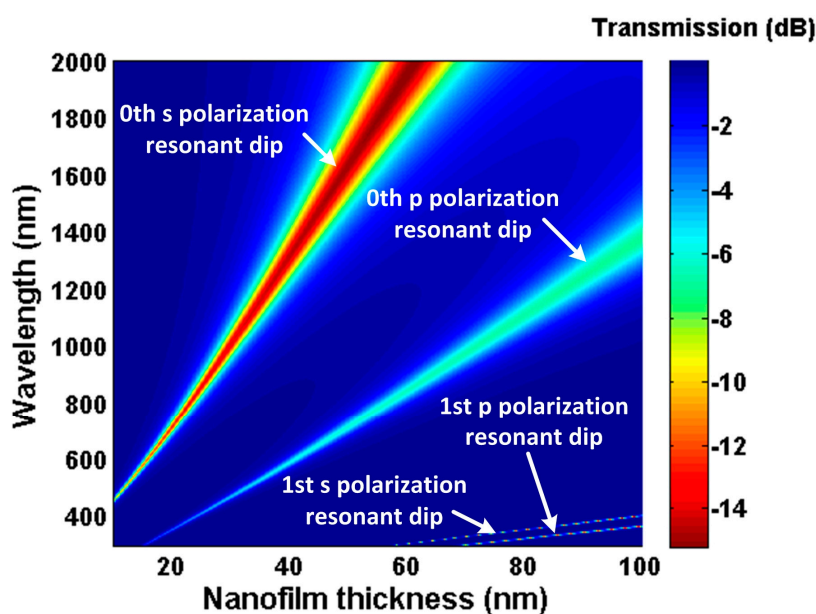


Figure 2. Transmission spectra as a function of the TiO₂ film thickness in water (1.33).

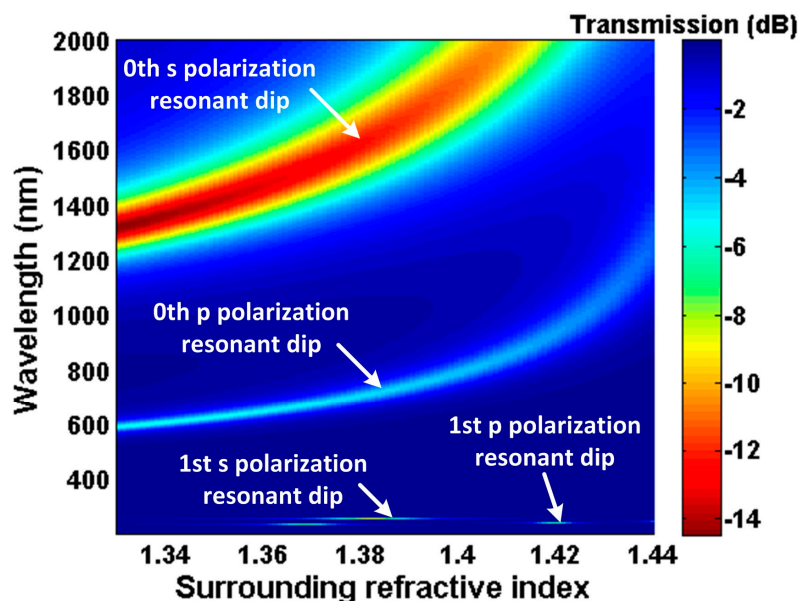


Figure 3. Transmission spectra as a function of surrounding refractive index (SRI) with $d = 40$ nm.

Meanwhile, temperature stability of the refractometer was studied. The thermo-optic coefficient of the TiO_2 nanofilm, the fiber cladding, and the water is $-4.2 \pm 0.7 \times 10^{-5}/^\circ\text{C}$ [24], $7.8 \times 10^{-6}/^\circ\text{C}$ [25], and $-9 \times 10^{-5}/^\circ\text{C}$ [26], respectively. These refractive indices have slight changes with the temperature fluctuation. According to Equation (4), we can calculate the sensitivity of the 0th resonant dip to temperature ($d = 40$ nm), which is $0.48 \text{ nm}/^\circ\text{C}$ for the s polarization resonant dip and $0.18 \text{ nm}/^\circ\text{C}$ for the p polarization resonant dip. When SRI changes by 0.002 RIU (the SRI step in the experiment), a resonant wavelength shift of 9.0 nm for the s polarization resonant dip and 3.6 nm for the p polarization resonant dip can be achieved. However, a change in temperature of 18.8°C is required to obtain the same amount of shift. Therefore, a shift in temperature by 1°C results in a change of the measured refractive index by 1×10^{-4} RIU.

3. Fabrication of Tapered Fiber Coated with TiO_2 Nanofilm

3.1. Adiabatic Tapered Fiber Fabrication

In this work, we used a heat-pulling system with oxyhydrogen flame to fabricate the adiabatic tapered optical fiber. The taper waist diameter and the total length are approximately $25 \mu\text{m}$ and 16 mm , respectively. The insertion loss of the pulled fiber taper is less than -1 dB .

3.2. TiO_2 Nanofilm Deposition

To deposit the nanofilm around the tapered fiber waist, ALD equipment (TFS 200, Beneq) was utilized. The tapered fibers were placed in a cylindrical reaction chamber whose diameter and height were 22 cm and 3 cm , respectively.

The reaction temperature was kept at 140°C . The two precursors (TiCl_4 and H_2O) and N_2 gas were valve-controlled and pulsed into the reaction chamber with the order of $\text{TiCl}_4\text{-N}_2\text{-H}_2\text{O-N}_2$. When TiCl_4 is introduced, the first half-reaction proceeds as $-\text{OH} + \text{TiCl}_4 \rightarrow -\text{OTiCl}_3 + \text{HCl}$. When all of the available OH-sites are reacted, the half-reaction stops. HCl gas is released as the by-product, and the surface changes from $-\text{OH}$ to $-\text{TiCl}$ groups. Then, the excess TiCl_4 and the HCl are purged away by N_2 . When H_2O is introduced, the second half-reaction proceeds as $-\text{TiCl} + \text{H}_2\text{O} \rightarrow -\text{TiOH} + \text{HCl}$. This half-reaction forms Ti-O bands, and the surface is $-\text{OH}$ groups, which creates sites for the reaction of the next deposition cycle. The excess H_2O and the HCl are purged away by N_2 . The monolayer TiO_2 film was deposited on the surface of the taper waist in 7 s. Repeating the deposition

cycle, the TiO_2 film can be deposited layer by layer. Due to the self-limiting growth mechanism, the monolayer thickness is almost the same in each deposition cycle, and the thickness of the final TiO_2 film can be precisely controlled through the number of deposition cycles.

The TiO_2 film deposited on the optical fibers was characterized using X-ray photoelectron spectroscopy (XPS) and scanning electron microscopy (SEM). Figure 4 shows the XPS results. The titanium and oxygen are registered respectively, which confirms that the TiO_2 film has been successfully deposited.

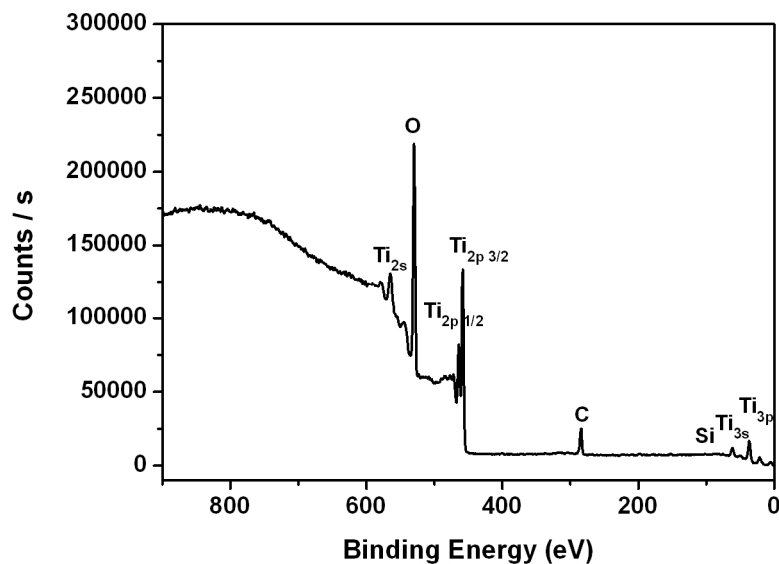


Figure 4. X-ray photoelectron spectroscopy (XPS) picture of optical fiber deposited with TiO_2 nanofilm.

Figure 5 shows an SEM image of the cross section of an optical fiber deposited with 3000 layers of TiO_2 film. In Figure 5, the thickness is approximately 113 nm, so the average thickness per layer is about 0.0377 nm.

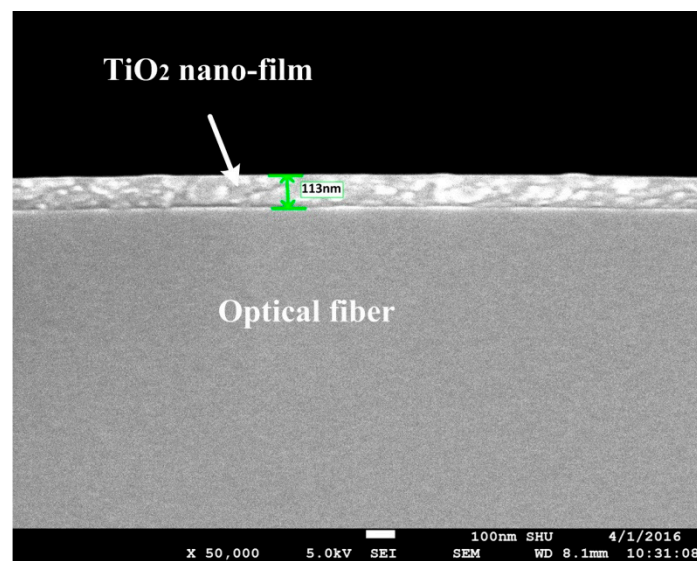


Figure 5. Scanning electron microscopy (SEM) picture of an optical fiber deposited with 3000 layers TiO_2 nanofilm.

4. Experiments and Results

With a broadband light source (NKT Photonics SuperK Compact, 500 nm–2400 nm) and two optical spectrum analyzers (AQ-6315A <600 nm–1700 nm>, AQ-6375 <1200 nm–2400 nm>), the transmission spectra of the tapered fiber with TiO₂ film thickness of 39.7 nm, 45.2 nm, and 50.9 nm were measured in air and in deionized water, as shown in Figure 6a,b, respectively. We observe that the 0th resonant dips shift to the longer wavelength and the bandwidth of the resonant spectra are markedly broadened as the TiO₂ film thickness increases, both in air and in deionized water. Moreover, for the TiO₂ film with the same thickness, the resonant wavelengths exhibit a red shift with switching from air to deionized water, which indicates that the TiO₂-coated adiabatic tapered fiber is sensitive to the change of SRI. Figure 6c shows that the shift of the resonant wavelength is linearly proportional to the nanofilm thickness. According to this relationship, we can set the deposition cycle to adjust the working point. The experimental results obtained in Figure 6c show good agreement with the theoretical results.

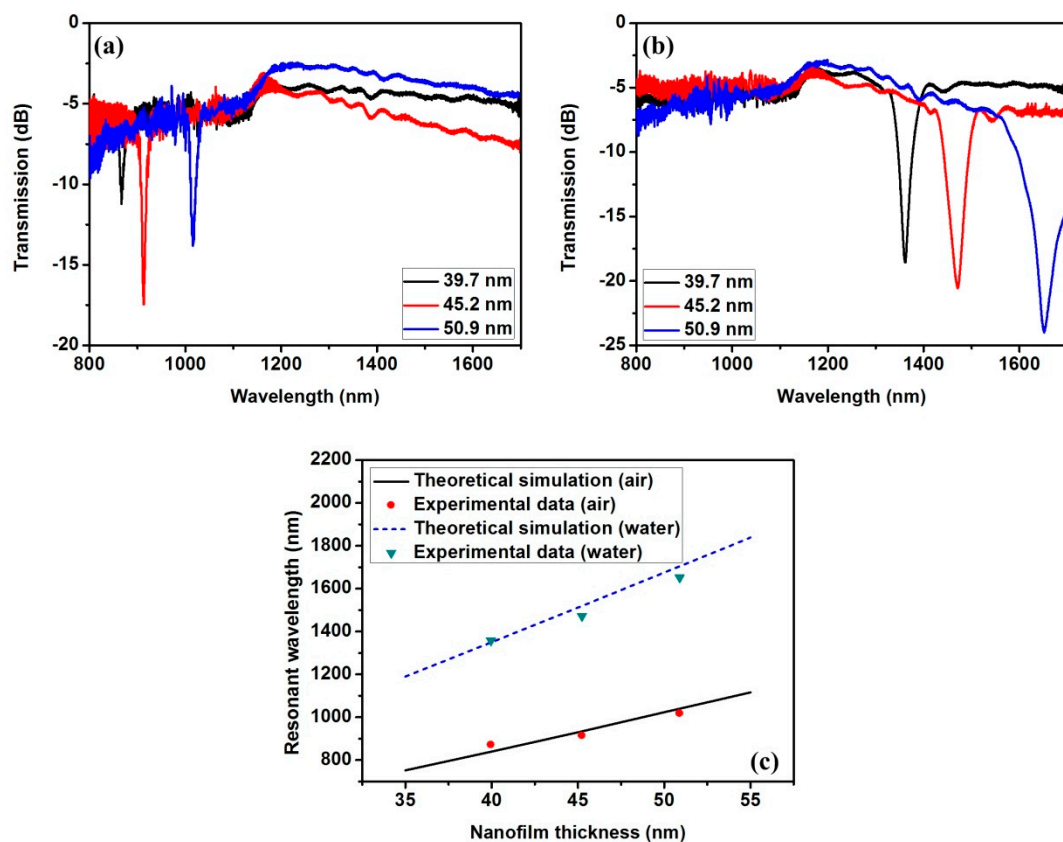


Figure 6. Transmission spectra obtained when the tapered fiber with TiO₂ thicknesses of 39.7, 45.2, and 50.9 nm are immersed in (a) air and (b) deionized water; and (c) resonant wavelength as a function of the TiO₂ film thickness.

In the sensing experiment for SRI, the fiber taper sensor head was fixed on a glass microscope slide, and liquid samples with different refractive indices were dropped on the sensor head. A mixture of glycerol and deionized water in different ratios was used as the liquid sample. The SRI is from 1.3373 to 1.3500, which was certified by using an Abbe refractometer with a resolution of 0.0001. The temperature around the sensor head was maintained at approximately 20 °C in order to minimize the SRI/temperature cross sensitivity. In addition, the sensor head was cleaned by deionized water and dried after each sample measurement.

Three sensors with TiO₂ film thickness of 39.7 nm, 45.2 nm, and 50.9 nm were fabricated and investigated. The transmission spectra versus SRI are shown in Figure 7a–c. As the SRI increases, all of the transmission spectra shift toward the longer wavelength. According to Equation (4), this relationship results from the decrease in the phase delay induced by the Goos–Hänchen shift in the total internal reflection on the nanofilm–surrounding interface. In addition, the shift amount increases gradually with the increase of nanofilm thickness. The reason is that the incident angle for the same order resonant dip will increase to satisfy the phase interference condition, which will lead to an increase in the Goos–Hänchen phase delay change rate according to the TIR feature [23]. Hence, a greater amount of shift can be obtained with increasing nanofilm thickness. Namely, the shift amount increases as the resonant wavelength shifts to a longer wavelength.

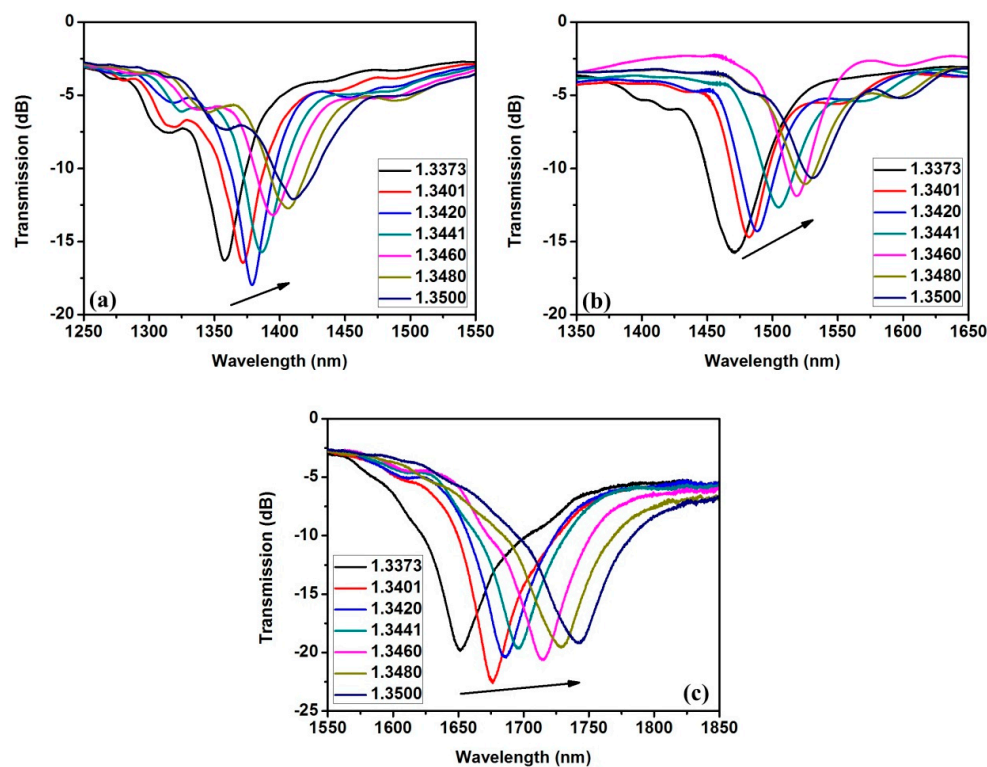


Figure 7. Transmission spectra shift with increasing SRI for different TiO₂ film thickness values. (a) 39.7 nm; (b) 45.2 nm; (c) 50.9 nm.

In Figure 8, we can also observe that the shift of the resonant wavelength is a linear function of the SRI. It shows that the sensitivity is enhanced for the sensor head with thicker nanofilms. The sensitivity of the tapered fiber with TiO₂ film thickness of 39.7 nm, 45.2 nm, and 50.9 nm are 4180 nm/RIU, 5116 nm/RIU, and 7096 nm/RIU, respectively. Moreover, compared with the tapered fiber coated with Al₂O₃ nanofilm where the maximum sensitivity is 6008 nm/RIU [13], the sensitivity of the tapered fiber coated with TiO₂ nanofilm has been improved, which results from the higher refractive index of TiO₂. These results agree with previous discussion that either increasing nanofilm thickness or increasing nanofilm refractive index can improve the sensitivity for the same order resonant dip.

The stability characteristic of the refractometer is also studied. The liquid sample with a refractive index of 1.3369 was dropped on the sensor head with a TiO₂ film thickness of 45.2 nm. The transmission spectrum was acquired every 2 min. In order to minimize the effect of liquid sample evaporation on the experimental results during a 70-min test, the sensor head was sealed in a small plastic box. As shown in Figure 9, the resonant wavelength fluctuates very little over time, and the Root Mean Square (RMS) value of the fluctuation is about 0.2 nm. The change in refractive index corresponding

to the measured wavelength fluctuation is 1.5×10^{-4} . The result indicates that the refractometer has good stability.

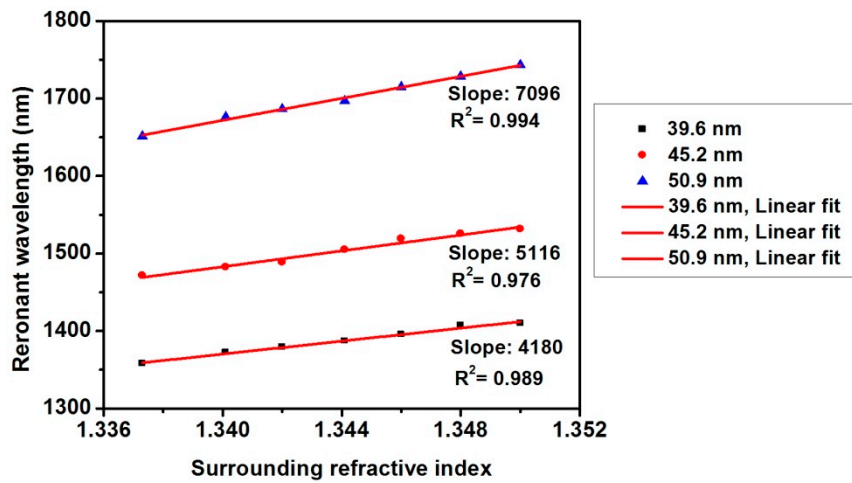


Figure 8. Relative resonant wavelength increases with increasing SRI for different TiO₂ film thickness.

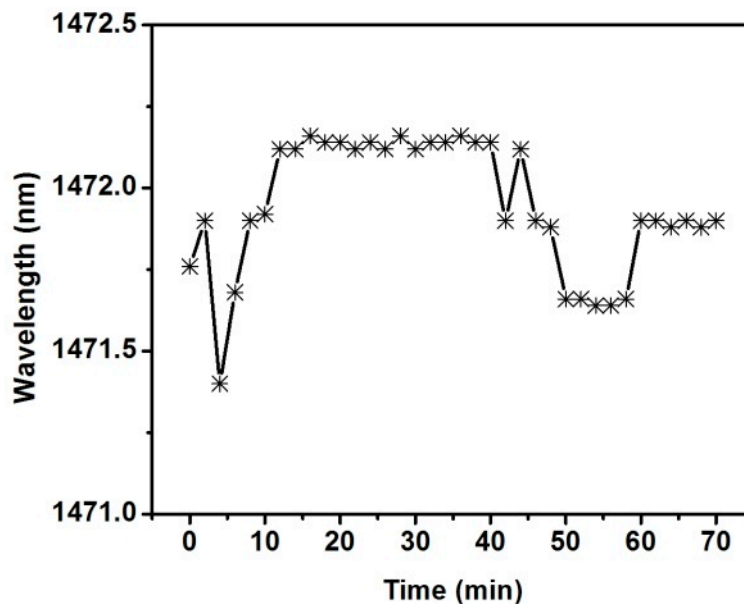


Figure 9. Resonant wavelength versus time.

5. Conclusions

In this paper, a TiO₂-coated adiabatic tapered optical fiber was fabricated by ALD technology. The fabricated devices show a red shift of their resonant wavelength as the SRI increases, which enables their use for SRI sensing purposes. Since the phase delay induced by the Goos–Hänchen shift has a significant impact on the resonant phase condition for the 0th s polarization resonant dip, high sensitivity for SRI can be obtained. Based on the advantages of ALD technology, tunable thickness of the TiO₂ nanofilm ensures precise control of the transmission spectrum. Moreover, the thickness also determines the sensitivity of the sensor. The experimental results demonstrate that the high sensitivity of 7096 nm/RIU in the range 1.3373–1.3500 can be obtained, which is better than Al₂O₃-coated adiabatic tapered fiber refractometers for the same order of resonant spectrum [13]. The results have proven that a higher refractive index nanofilm permits the achievement of improved sensitivity. In general,

a refractometer based on a TiO₂ nanofilm is more suitable for biochemical applications due to the advantages of TiO₂, such as high refractive index, lack of toxicity, and good biocompatibility.

Acknowledgments: This project was funded by the Natural Science Foundation of China (61275090, 61422507, 61227012), National key research and development program of China (2016YFF0100603), and Innovation Program of Shanghai Municipal Education Commission (14ZZ093).

Author Contributions: Shan Zhu, Fufei Pang and Tingyun Wang conceived and designed the sensor; Shan Zhu performed simulation and experimental works; Fang Zou helped with simulation; Jianxiang Wen and Qiang Guo contributed with TiO₂ material and ALD equipment debugging; Shan Zhu and Fufei Pang analyzed the data and wrote the paper; Sujuan Huang offered help in the process of writing; Tingyun Wang reviewed the manuscript for scientific content and supervised the entire project.

Conflicts of Interest: The authors declare no conflict of interest.

References

1. Shu, X.; Zhang, L.; Bennion, I. Sensitivity characteristics of long-period fiber gratings. *J. Light. Technol.* **2002**, *20*, 255–266.
2. Villatoro, J.; Monzón-Hernández, D.; Talavera, D. High resolution refractive index sensing with cladded multimode tapered optical fibre. *Electron. Lett.* **2004**, *40*, 106–107. [[CrossRef](#)]
3. Rees, N.D.; James, S.W.; Tatam, R.P.; Ashwell, G.J. Optical fiber long-period gratings with Langmuir-Blodgett thin-film overlays. *Opt. Lett.* **2002**, *27*, 686–688. [[CrossRef](#)] [[PubMed](#)]
4. Del Villar, I.; Matías, I.; Arregui, F.; Lalanne, P. Optimization of sensitivity in Long Period Fiber Gratings with overlay deposition. *Opt. Express* **2005**, *13*, 56–69. [[CrossRef](#)] [[PubMed](#)]
5. Zou, F.; Liu, Y.; Deng, C.; Dong, Y.; Zhu, S.; Wang, T. Refractive index sensitivity of nano-film coated longperiod fiber gratings. *Opt. Express* **2015**, *23*, 1114–1124. [[CrossRef](#)] [[PubMed](#)]
6. Zhao, Y.; Pang, F.; Dong, Y.; Wen, J.; Chen, Z.; Wang, T. Refractive index sensitivity enhancement of optical fiber cladding mode by depositing nanofilm via ALD technology. *Opt. Express* **2013**, *21*, 26136–26143. [[CrossRef](#)] [[PubMed](#)]
7. Xue, L.; Yang, L. Sensitivity enhancement of RI sensor based on SMS fiber structure with high refractive index overlay. *J. Light. Technol.* **2012**, *30*, 1463–1469.
8. Diez, A.; Andres, M.V.; Cruz, J.L. Hybrid surface plasma modes in circular metal-coated tapered fibers. *J. Opt. Soc. Am. A* **1999**, *16*, 2978–2982. [[CrossRef](#)]
9. Lin, H.Y.; Huang, C.H.; Cheng, G.L.; Chen, N.K.; Chui, H.C. Tapered optical fiber sensor based on localized surface plasmon resonance. *Opt. Express* **2012**, *20*, 21693–21701. [[CrossRef](#)] [[PubMed](#)]
10. Zamarreno, C.R.; Lopez, S.; Hernández, M.; Del Villar, I.; Matías, I.R.; Arregui, F.J. Resonance-based refractometric response of cladding-removed optical fibers with sputtered indium tin oxide coatings. *Sens. Actuators B Chem.* **2012**, *175*, 106–110. [[CrossRef](#)]
11. Zubiarte, P.; Zamarreño, C.R.; Del Villar, I.; Matías, I.R.; Arregui, F.J. High sensitive refractometers based on lossy mode resonances (LMRs) supported by ITO coated D-shaped optical fibers. *Opt. Express* **2015**, *23*, 8045–8050. [[CrossRef](#)] [[PubMed](#)]
12. Hernández, M.; Del Villar, I.; Zamarreño, C.R.; Arregui, F.J.; Matías, I.R. Optical fiber refractometers based on lossy mode resonances supported by TiO₂ coatings. *Appl. Opt.* **2010**, *49*, 3980–3985. [[CrossRef](#)] [[PubMed](#)]
13. Zhu, S.; Pang, F.; Huang, S.; Zou, F.; Dong, Y.; Wang, T. High sensitivity refractive index sensor based on adiabatic tapered optical fiber deposited with nanofilm by ALD. *Opt. Express* **2015**, *23*, 13880–13888. [[CrossRef](#)] [[PubMed](#)]
14. Socorro, A.B.; Del Villar, I.; Corres, J.M.; Arregui, F.J.; Matías, I.R. Spectral width reduction in lossy mode resonance-based sensors by means of tapered optical fibre structures. *Sens. Actuators B Chem.* **2014**, *200*, 53–60. [[CrossRef](#)]
15. Pilla, P.; Malachovská, V.; Borriello, A.; Buosciolo, A.; Giordano, M.; Ambrosio, L.; Cutolo, A.; Cusano, A. Transition mode long period grating biosensor with functional multilayer coatings. *Opt. Express* **2011**, *19*, 512–526. [[CrossRef](#)] [[PubMed](#)]
16. Kim, H.; Lee, H.; Maeng, W. Applications of atomic layer deposition to nanofabrication and emerging nanodevices. *Thin Solid Films* **2009**, *517*, 2563–2580. [[CrossRef](#)]

17. Smietana, M.; Mysliwiec, M.; Mikulic, P.; Witkowski, B.S.; Bock, W.J. Capability for fine tuning of the refractive index sensing properties of long-period gratings by atomic layer deposited Al₂O₃ overlays. *Sensors* **2013**, *13*, 16372–16383. [[CrossRef](#)]
18. Krogulski, K.; Śmietana, M.; Michalak, B.; Dębowska, A.K.; Wachnicki, Ł.; Gierałtowska, S.; Godlewski, M.; Szymańska, M.; Mikulic, P.; Bock, W.J. Effect of TiO₂ nano-overlays deposited with atom on refractive index sensitivity of long-period gratings. In Proceedings of the 8th International Conference on Sensing Technology, Liverpool, UK, 2–4 September 2014; pp. 573–577.
19. Roussey, M.; Descrovi, E.; Häyrynen, M.; Angelini, A.; Kuittinen, M.; Honkanen, S. One-dimensional photonic crystals with cylindrical geometry. *Opt. Express* **2014**, *22*, 27236–27241. [[CrossRef](#)] [[PubMed](#)]
20. Love, J.D.; Henry, W.M.; Stewart, W.J.; Black, R.J.; Lacroix, S.; Gonthier, F. Tapered single-mode fibres and devices part 1: Adiabaticity criteria. *IEEE Proc. J* **1991**, *138*, 343–354. [[CrossRef](#)]
21. Villatoro, J.; Monzón-Hernández, D.; Mejía, E. Fabrication and modeling of uniform-waist single-mode tapered optical fiber sensors. *Appl. Opt.* **2003**, *42*, 2278–2283. [[CrossRef](#)] [[PubMed](#)]
22. Yariv, A.; Yeh, P. *Photonics: Optical Electronics in Modern Communications*, Chinese Language 6th ed.; Oxford University Press, Inc.: Oxford, UK, 2009; pp. 149–151.
23. Kokubun, Y. *Optical Engineering*; Science Press: Beijing, China, 2002. (In Chinese)
24. Saleem, M.R.; Honkanen, S.; Turunen, J. Thermal properties of TiO₂ films fabricated by atomic layer deposition. *IOP Conf. Ser. Mater. Sci. Eng.* **2014**, *60*, 012008. [[CrossRef](#)]
25. Singh, A.; Engles, D.; Sharma, A.; Singh, M. Temperature sensitivity of long period grating in SMF-28 fiber. *Optik* **2014**, *125*, 457–460. [[CrossRef](#)]
26. Georges, J.; Paris, T. Influence of the Soret effect on the analytical signal in cw-laser thermal lens spectrometry of micellar solutions. *Anal. Chim. Acta* **1999**, *386*, 287–296. [[CrossRef](#)]



© 2016 by the authors; licensee MDPI, Basel, Switzerland. This article is an open access article distributed under the terms and conditions of the Creative Commons Attribution (CC-BY) license (<http://creativecommons.org/licenses/by/4.0/>).